Unified cluster expansion method applied to the configurational thermodynamics of cubic $Ti_{1-x}Al_xN$

B. Alling,[1,*] A. V. Ruban,[2] A. Karimi,[3] L. Hultman,[1] and I. A. Abrikosov[1]

[1]*Department of Physics, Chemistry and Biology (IFM), Linköping University, SE-58183 Linköping, Sweden*

[2]*Department of Materials Science and Engineering, Royal Institute of Technology (KTH), SE-10044 Stockholm, Sweden*

[3]*Institute of Condensed Matter Physics (IPMC), École Polytechnique Fédérale de Lausanne (EPFL), CH-1015 Lausanne, Switzerland*

(Received 12 December 2010; revised manuscript received 28 January 2011; published 25 March 2011)

We study the thermodynamics of cubic $Ti_{1-x}Al_xN$ using a unified cluster expansion approach for the alloy problem. The purely configurational part of the alloy Hamiltonian is expanded in terms of concentration- and volume-dependent effective cluster interactions. By separate expansions of the chemical fixed lattice, and local lattice relaxation terms of the ordering energies, we demonstrate how the screened generalized perturbation method can be fruitfully combined with a concentration-dependent Connolly-Williams cluster expansion method. Utilizing the obtained Hamiltonian in Monte Carlo simulations we access the free energy of $Ti_{1-x}Al_xN$ alloys and construct the isostructural phase diagram. The results show striking similarities with the previously obtained mean-field results: The metastable c-TiAlN is subject to coherent spinodal decomposition over a larger part of the concentration range, e.g., from $x \geqslant 0.33$ at 2000 K.

DOI: 10.1103/PhysRevB.83.104203 PACS number(s): 64.60.Cn, 71.23.−k

I. INTRODUCTION

Metastable cubic $Ti_{1-x}Al_xN$ solid solutions[1–3] are one of the most widely used classes of hard protective coating materials.[4] The addition of Al to TiN coatings has been shown to result in better oxidation resistance[2] and retained or even increased hardness at temperatures reached in for cutting tool applications.[5] Al-rich cubic TiAlN films demonstrates particularly good properties. The age-hardening mechanism has been shown to be due to a coherent isostructural spinodal decomposition of the as-deposited cubic $Ti_{1-x}Al_xN$ solid solutions into TiN (or Ti-rich TiAlN) and cubic AlN domains.[5,6] The existence of an energetic demixing driving force has been proven theoretically by means of first-principles calculations[7,8] and explained to be primarily due to an electronic structure mismatch effect that is particularly strong for the Al-rich compositions.[8]

The isostructural phase diagram, derived theoretically within the mean-field approximation,[8] shows an almost complete miscibility gap between TiN and c-AlN at temperatures of relevance for cutting tool applications, around 1300 K. According to these estimates, the composition region displaying spinodal decomposition extends from $x = 0.25$ to $x = 0.99$ at this temperature[8] but could be further extended when subjected to cutting-induced pressure.[9,10] However, the mean-field approximation neglects the effect of short range order or clustering and is known to overestimate the critical temperatures.[11] The qualitative importance of local clustering in TiAlN for the isostructural decompositions as well as for the maximum amount of Al possible to solve in the cubic phase before appearance of wurtzite AlN during synthesis has been noted in a number of articles.[7,8,12]

Here, we investigate the clustering thermodynamics of cubic TiAlN using an accurate statistical mechanics analysis beyond the mean-field approximation. In doing so we use concentration- and volume-dependent effective cluster interactions, which are devised by a here-proposed combination of two complementary methods: the generalized perturbation method (GPM)[13] and the structure inverse or Connolly-Williams cluster expansion (CE) method.[14] In this way we are able to provide accurate mapping of the complex interatomic interactions onto an Ising-type Hamiltonian, which can then be used in Monte Carlo calculations of the configurational part of the free energy and its contribution to the isostructural phase diagram of the system.

II. ALLOY HAMILTONIAN

In a previous investigation of the c-$Ti_{1-x}Al_xN$ system, the electronic structure and, as a consequence, mixing energy of these alloys were found to exhibit complicated behavior, which could not be captured by a simple regular solution model. Such behavior of the system, and the changes of its thermodynamic properties with concentration, is related to a gradual electronic structure transition due to bond cutting of the next-to-nearest-neighbor (metal sublattice nearest-neighbor) Ti-Ti bonds of t_{2g} character, eventually leading to isolated and localized states in a semiconducting AlN-rich matrix.[8] This is in fact exactly the case where the concentration-independent (grand canonical) cluster expansion breaks down: The nature of the Ti-Ti interaction in the metallic state and in the semiconductor state differ.

Therefore, the concentration-dependent expansion of the configurational energy is the only reasonable choice for the alloy Hamiltonian in TiAlN. In general, such a Hamiltonian is defined as

$$\begin{aligned}\mathcal{H}_{\text{conf}} = &\frac{1}{2}\sum_p V_p^{(2)}(x)\sum_{i,j\in p}\delta c_i\delta c_j \\ &+\frac{1}{3}\sum_t V_t^{(3)}(x)\sum_{i,j,k\in t}\delta c_i\delta c_j\delta c_k \\ &+\frac{1}{4}\sum_q V_q^{(4)}(x)\sum_{i,j,k,l\in q}\delta c_i\delta c_j\delta c_k\delta c_l+\cdots, \quad (1)\end{aligned}$$

where $V_\alpha^{(n)}(x)$ are the n-site effective cluster interactions for specific cluster α and the concentration of Al x; and $\delta c_i = c_i - x$ are the concentration fluctuation variables defined in

terms of the occupation numbers c_i, which takes on values 1 or 0, if Al or Ti atom occupies site i, respectively.

The Hamiltonian in Eq. (1) takes care only of the configurational part, so the total alloy Hamiltonian can be obtained if either the total energy of a random alloy or its mixing enthalpy (in this case at zero pressure), $\Delta H_{\rm mix}(x) = E_{\rm tot}(x) - xE_{\rm tot}(x=0) - (1-x)E_{\rm tot}(x=1)$, are added to the configurational Hamiltonian. In this work we use the latter for convenience:

$$\mathcal{H}_{\rm all} = \Delta H_{\rm mix}(x) + \mathcal{H}_{\rm conf}. \tag{2}$$

Equation (2) follows from the fact that the configurational energy of a random alloy in Eq. (1) is exactly zero, since in this case $\langle \delta c_i \delta c_j \cdots \delta c_k \rangle = \langle \delta c_i \rangle \langle \delta c_j \rangle \cdots \langle \delta c_k \rangle = 0$. Let us note that in the case of the concentration-independent cluster expansion, the mixing enthalpy is reexpanded in terms of the corresponding effective cluster interactions.

The next important point is the separation of the effective cluster interactions in the Hamiltonian of Eq. (1) into chemical part, defined as the situation with all atoms sitting on fixed ideal lattice points in the absence of any local relaxations, and the additional relaxation part, which takes care of the rest of the energy, associated with local lattice relaxations specific for a given atomic configuration:

$$V_\alpha^{(n)} = V_\alpha^{(n)-{\rm fix}} + V_\alpha^{(n)-{\rm rel}}, \tag{3}$$

where $V_\alpha^{(n)-{\rm fix}}$ and $V_\alpha^{(n)-{\rm rel}}$ are the chemical fixed lattice and relaxation part of n-site interaction $V_\alpha^{(n)}$, respectively.

With this separation one can gain an important advantage if there is an efficient way to get the chemical part of the interactions. This part may exhibit nontrivial behavior and nonlinear concentration dependence, induced, for instance, by the electronic structure effect as demonstrated in Ref. 8. On the other hand, at least in the system studied here, the local lattice relaxations, although important, show a very smooth behavior as a function of concentration. In fact, in TiAlN the latter originates to a large extent from the relaxation of nitrogen atoms and can be well explained by the independent sublattice model, given by a simple one-parameter equation.[8] In this work, however, we aim for a more detailed description also of the relaxation part of the problem.

The effect of thermal expansion as well as vibrational entropy and electronic excitations are neglected in this work. We do not believe that thermal expansion has a large impact on the here calculated properties in the temperature regions that have any practical relevance. This is so since in a test calculation, the strongest of our obtained cluster interactions in $Ti_{0.5}Al_{0.5}N$ decreased with only about 2% when the lattice parameter was expanded with 2%. This tested expansion is substantially larger than the experimentally observed for TiN at 1692 K: 1.3% (with respect to room temperature).[15] Thus, in the present system, the hard ceramic type bondings makes vibrational effects less important at the temperatures of relevance, especially with respect to the very strong configurational energetics, to be shown below. Of course, for the extreme temperatures needed to close the isostructural miscibility gap, vibrational effects are large, e.g., TiN melts at about 3500 K.[16] However, this region is included only for completeness and to discuss consequences of the configurational modeling scheme and not to be used for any direct comparisons with experiments.

III. TOTAL ENERGY CALCULATIONS AND MIXING ENTHALPIES

The total energy calculations were done using two different electronic structure methods. First, the electronic structure and total energies of random c-$Ti_{1-x}Al_xN$ alloys have been calculated by the exact muffin-tin orbitals (EMTO) method in the coherent potential approximation (CPA).[17,18] The CPA method, however, neglects local lattice relaxation effects and, therefore, to get the relaxation energy contribution, we combine it with supercell calculations. In the latter, the projector augmented wave (PAW)[19] method has been used as implemented in the Vienna *ab initio* simulation package (VASP)[20,21] to calculate the energies of supercells modeling the random state. These are created by closely matching the pair correlation functions on the coordination shells where the effective cluster interactions are strongest to the values in real random alloys as described in Ref. 8. This procedure is an extension of the strategy suggested by Zunger *et al.*[22] in their design of so-called special quasirandom structures (SQS)[22] but is based on a rigorous condition for the validity of the usage of a supercell for modeling the random state.[23,24] Although we do not use the originally suggested small special SQS structures in this work, we use the abbreviation SQS for our randomlike supercells in line with the terminology in previous publications. A comparison between SQS and Connolly-Williams cluster expansion calculations was recently presented by Ghosh *et al.* for, e.g., Al-Ti intermetallics.[25]

Internal coordinates and volume were relaxed for each of the SQS structures while we neglected the shape relaxation, which should be absent in a real random alloy due to the preservation of the $B1$ symmetry on average. In addition, 100 ordered structures for the concentrations $x = 0.25, 0.375, 0.5, 0.625$, and 0.75 are considered for the cluster expansion of the lattice relaxation energies. The ordered structures have between 4 and 16 metal atoms and are constructed by multiplying the unit cell in the [001], [011], [111], and [211] directions, assuring that they all have unique combinations of the pair correlation functions at the first two coordination shells. Their energies have been calculated using the PAW method, allowing for relaxation of all internal coordinates and shape, while their volumes were kept fixed at the equilibrium volume of the corresponding SQS. All calculations have been done using the generalized gradient approximation (GGA)[26] for electronic exchange-correlation effects within the density functional framework. The details of the calculations are the same as in Ref. 8.

Thus, the mixing enthalpies, at zero pressure, of the random alloys, $\Delta H_{\rm mix}(x)$ in Eq. (2), were calculated using the EMTO-CPA method for its fixed lattice part and the PAW-SQS method for the relaxation part, the latter decreasing the positive mixing enthalpies of the alloys with about one-third.[8] Note that it was shown that the two methods gave very similar results for fixed lattice calculations.[8]

The mixing enthalpies (at zero pressure) of the SQS structures as well as obtained with the CPA method combined with an interpolation of the SQS lattice relaxation energies are discussed in Sec. IV C.

IV. EFFECTIVE CLUSTER INTERACTIONS

A. Effective fixed-lattice chemical interactions

The effective fixed-lattice chemical interactions were obtained by the screened GPM.[27–29] The starting point of this method is the electronic structure of a random alloy at a given concentration and external conditions. The latter is usually obtained in the CPA, which provides the effective medium in order to calculate the energy response of the system to a particular effective perturbation by the proper expansion of the one-electron energy term.[11,13] This part is calculated within the EMTO method but using the slightly smaller lattice parameters from the PAW calculations for consistency with the derivation of the relaxation part of the interactions. The effect on the interactions of this small lattice parameter difference, which is less then 1%, is, however, almost negligible. In the case of DFT formulation one then has to add an additional electrostatic contribution following the force theorem.[27–29] The latter contributes only to the effective pair interactions and is determined in supercell calculations, allowing the evaluation of the screening density in the corresponding random alloy. In this work this screened electrostatic contribution was obtained in very large randomlike supercell calculations by the locally self-consistent Green's function (LSGF) method.[23,30]

The screened GPM was used to calculate (i) the effective pair interactions up to the 30th coordination shell, (ii) all the three-site interactions in which the sides correspond up to the fifth coordination shell, and (iii) all the four-site interactions with the edges up to the fourth coordination shell. In addition, we also calculated one specific, more distant, four-site interaction, which is known to give quite large contributions to the configurational energetics due to its specific geometry. It is the interaction for the four-site cluster along the line of the [110] direction. The strongest of the multisite interactions are shown in the lower panels of Fig. 1 where the interaction index is given by the coordination shell numbers of the sides of the corresponding cluster. In the case of the four-site interactions, the order of the indexes are important, so we make the following choice: the first four indexes are the coordination shells of the sides of a closed loop through all four sites, and the last two are the coordination shells of the remaining sides of the cluster.

It is clear that the most important effective chemical interactions of the fixed lattice are the nearest- and next-to-nearest-neighbor pair interactions. They are negative, favoring clustering, and show a strong nonlinear decrease with Al concentration. The three-site and four-site interactions are all rather weak for concentrations up to about $x \leqslant 0.60$. However, they increase sharply for higher Al content. This is a signature of the gradual electronic transition where Ti $3d$ states with t_{2g} symmetry, in the absence of Ti nearest (metal site) neighbors, becomes isolated in a semiconducting AlN matrix, as discussed above. It is also the reason why it would be dangerous to expand the configurational energy of c-TiAlN using concentration-independent interaction potentials.

There are two major approximations behind the screened GPM method: the CPA and the atomic sphere approximation (ASA). The CPA neglects the local environment effects in the electronic structure of a random alloy. The ASA errors come in different ways, but the most significant one is related

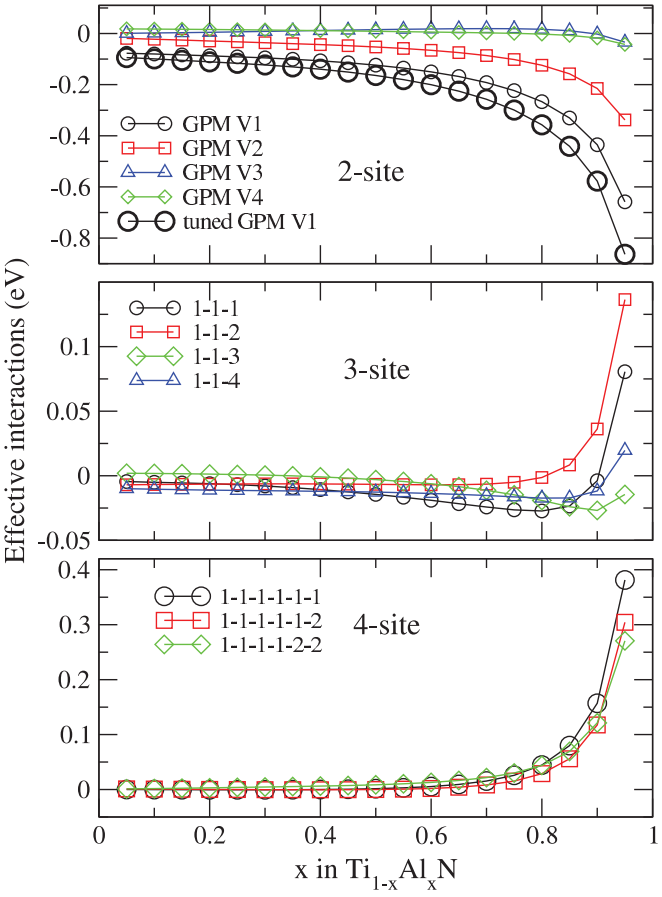

FIG. 1. (Color online) The strongest of the chemical fixed lattice effective two-, three-, and four-site interactions as a function of Al content obtained by the GPM method together with the tuned pair interaction at the first coordination shell.

to the screened Coulomb interactions, which are defined in the specific geometry of the atomic spheres. Both these approximations most strongly affect the interactions at the first few coordination shells.

In this work, we use the fixed-lattice results from the calculated mixing energies of the ordered structures to *tune* the GPM interactions. This is done by assuming that the long-range pair interactions and the multisite interactions are well described by the GPM and then cluster expand the remaining part of the ordering energies corresponding to the short-ranged pair clusters using the concentration-dependent CE method. An equivalent viewpoint is that the *errors* of the GPM is cluster expanded.

In our case it turns out that it is enough to tune only one pair interaction at the first coordination shell to obtain good agreement between the ordering energies from the cluster expansion and direct total-energy calculations. It is interesting to note that the tuning results in an almost concentration-independent scaling of the GPM nearest-neighbor interaction by a factor of 1.26–1.28. This tuned-GPM interaction is shown with large circles in the top panel of Fig. 1. If we allow for simultaneous tuning also of the next-to-nearest-neighbor pair interactions, we obtain for this shell almost the original GPM value (scaling factor of $\approx$1), clearly indicating the validity of our assumption about the short-

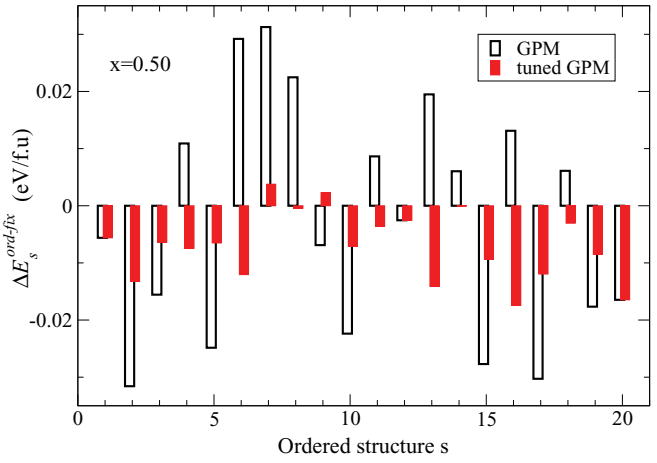

FIG. 2. (Color online) The error in the GPM and tuned-GPM descriptions of the fixed lattice part of the ordering energies of the 20 structures considered for $Ti_{0.5}Al_{0.5}N$. The average magnitude of the errors are 16.9 meV/f.u. using the GPM and 7.5 meV/f.u. using the tuned GPM.

range nature of the GPM inaccuracies. Of course, for other systems, the tuning procedure could possibly be extended to a few more shells for the obtaining of excellent fixed-lattice interactions.

Figure 2 shows the magnitude of the difference between the fixed-lattice ordering energies obtained with the direct PAW calculations, on the one hand, and the pure screened GPM and tuned screened GPM interactions, respectively, on the other. This difference can be expressed as

$$\Delta E^{s-\mathrm{fix}} = E^{s-\mathrm{fix}} - E^{\mathrm{SQS}-\mathrm{fix}} - \sum_f V_f^{(n)-\mathrm{fix}}\left[\xi_f^{(n)-s} - \xi_f^{(n)-\mathrm{SQS}}\right], \quad (4)$$

where $\xi_f^{(n)-s} = \langle \delta c_i \delta c_k \ldots \delta c_k \rangle_f$ are the correlation functions for figure f for the alloy having structure s.

Given the large total spread in ordering energies, which is more than 250 meV/f.u. for the structures with $x = 0.5$ considered here, the pure GPM potentials perform reasonably well. But by using the tuning scheme, the accuracy becomes very good. The average absolute value of the difference is reduced from 16.9 meV/f.u. for the pure GPM to 7.5 meV/f.u. using the tuned GPM. We note that a certain part of the remaining small error after the tuning comes from a constant shift in ordering energies. Such a small constant shift does not necessarily influence the description of energy differences between configurations treated in a statistical mechanics simulations.

B. Cluster expansion of the lattice relaxation energy

The relaxation term of the effective interactions were obtained by the concentration dependent Connolly-Williams CE method for the relaxation part of the energies of the ordered structures. The relaxation energy is defined for each structure as the energy difference between the situation where all atoms are sitting on ideal lattice points and when they have been allowed to relax to their equilibrium (eq) positions: $E^{s-\mathrm{rel}} = E^{s-\mathrm{eq}} - E^{s-\mathrm{fix}}$.

To obtain the $V_\alpha^{(n)-\mathrm{rel}}(x)$ we use a least-squares method to minimize the sum of the squares of the difference between the relaxation part of the ordering energies obtained with the Ising Hamiltonian and direct DFT calculations:

$$\Delta E^{s-\mathrm{rel}} = E^{s-\mathrm{rel}} - E^{\mathrm{SQS}-\mathrm{rel}} - \sum_f V_f^{(n)-\mathrm{rel}}\left[\xi_f^{(n)-s} - \xi_f^{(n)-\mathrm{SQS}}\right]. \quad (5)$$

Of course, also our cluster expansion faces the standard obstacles of the structure inversion method. However, we have a much easier job as compared to the conventional cluster expansion since we have separated out the complex chemical fixed-lattice term and only expand a part of the total ordering energies. Furthermore, judging from the shape of the relaxation energies of the SQS structures in Ref. 8, this part shows no sign of peculiar concentration dependence. Instead, it was shown that the local lattice relaxations in TiAlN is primarily due to relaxation of nitrogen atoms positioned between metal atoms of differing chemical type, an effect mostly depending on the pair correlation function on the second metal coordination shell.[8] In comparison, lattice mismatch gives a quite small contribution to the relaxation energies since pure TiN ($a_{\mathrm{PAW}} = 4.255$ Å) and c-AlN ($a_{\mathrm{PAW}} = 4.07$ Å) are rather close in lattice spacing.

For all considered concentrations, we have tested different cluster bases with up to 12 terms, including pair interactions up to the 15:th coordination shell, as well as short-ranged (up to the first and second coordination shells) three- and four-site interactions. Our conclusion is that the expansion based on the six pair interactions at the 1st, 2nd, 4th, 6th, 8th, and 10th shells gives a very good description of the relaxation energies for all concentrations. The inclusion of additional clusters, including multisite ones, in the expansion gives only minor improvements. Furthermore, the obtained relaxation interactions depend quite weakly on the concentration, in line with the findings in Ref. 8. We thus perform a linear regression to the obtained values to get the relaxation interactions for each concentration (in steps of $\Delta x = 0.05$) to be used in the statistical mechanics simulation.

The three strongest relaxation interaction parameters, the pair interactions on the 2nd, 4th, and 8th coordination shells, are shown in Fig. 3 as functions of concentration together with the linear regression values used in the Monte Carlo simulations. One can see that the strongest relaxation interaction, $V_2^{(2)-\mathrm{rel}}$ is positive, favoring ordering and corresponding to the relaxation of the nitrogen positions between metal atoms of different kinds, in line with Ref. 8. For all the relaxation interactions the linear regression fits well with the obtained values. Nevertheless, we double checked both ordering-energy calculations and statistical simulations using both the direct values and the values from the linear regression. The differences for the results were negligible. Note that all the relaxation interactions are rather weak compared to the first fixed lattice interaction $V_1^{(2)-\mathrm{fix}}$, especially in Al-rich alloys. But at lower Al content, on the other hand, the relaxation interactions become relatively more important.

The situation at $x = 0.5$ is shown in Fig. 4, where the pure GPM pair interactions are plotted with open black circles, the relaxation interactions are shown with solid red squares, and

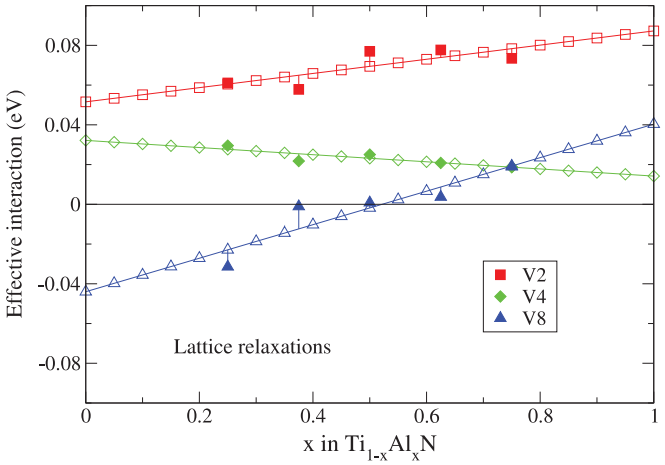

FIG. 3. (Color online) The three strongest relaxation interactions: pair interactions on the 2nd, 4th, and 8th coordination shells, as a function of Al content obtained by the the Connolly-Williams cluster expansion method (solid symbols). The linear regression values used in the Monte Carlo simulations are shown with open symbols. Note the different scale on the y axis as compared to the fixed-lattice chemical interactions shown in Fig. 1.

the resulting total pair interactions, including the tuning of the fixed-lattice interactions, are shown with large, bold circles.

C. Evaluation of the effective interactions

The top panel of Fig. 5 shows the mixing enthalpies (at zero pressure) of the SQS structures and as obtained using the CPA-method combined with an interpolation of the SQS lattice relaxation energies. Also shown are the mixing energies of the 100 ordered structures used in our cluster expansion procedure. The effective cluster interactions have been tested to produce the ordering energies of the considered 100 structures. The results are shown in the lower panel of

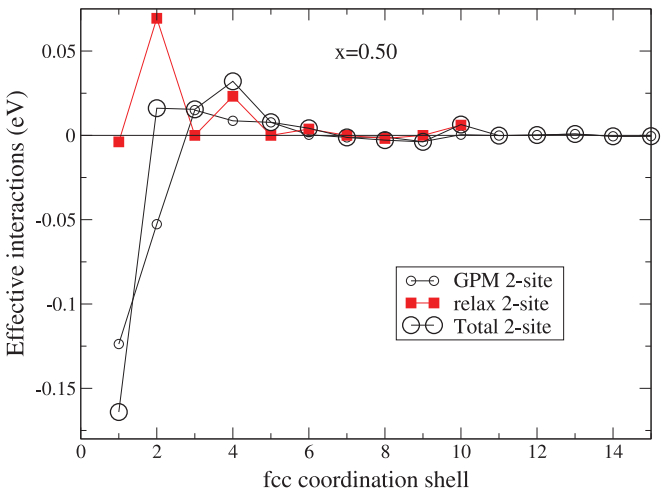

FIG. 4. (Color online) The effective cluster interactions used for the composition $Ti_{0.5}Al_{0.5}N$. Pure GPM interactions are shown by small open circles, and lattice relaxation interactions are shown by solid squares. The total effective pair interactions, $V_p^{(2)}$, including also the tuning of the fixed-lattice interaction on the first coordination shell, are shown with large circles.

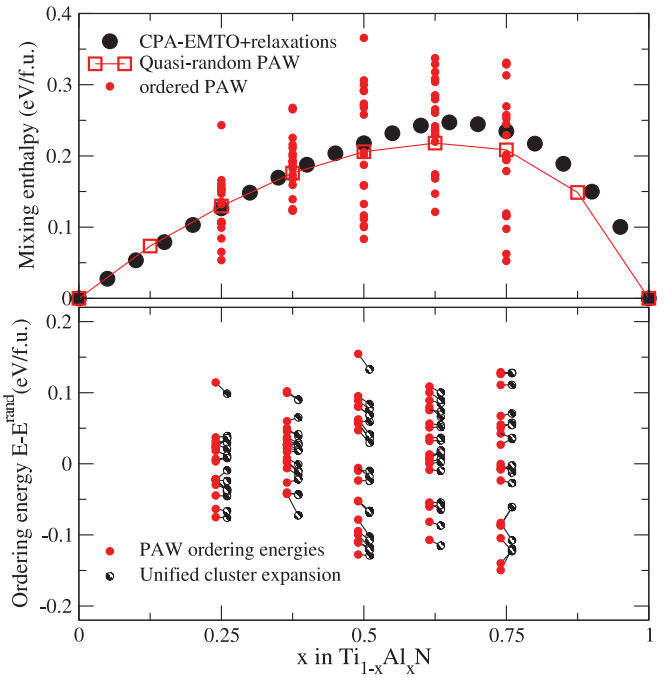

FIG. 5. (Color online) (Top panel) Mixing enthalpies of $Ti_{1-x}Al_xN$ random alloys calculated with the CPA-EMTO method (complimented with relaxation energies) and with the PAW-SQS method. Also shown are the mixing energies (at the SQS volumes) for 100 ordered structures. (Lower panel) The ordering energies of the 100 different $Ti_{1-x}Al_xN$ ordered structures. The values of direct PAW calculations are shown with solid red circles. The unified cluster expansion is shown with striped black circles.

Fig. 5. The ordering energies from the direct calculations are based on the comparison with the SQS energies but adjusted for the small but nonzero correlation functions of those supercells, $\xi_f^{(n)-\mathrm{SQS}}$ according to

$$E_{\mathrm{direct}}^{s-\mathrm{ord}} = E_{\mathrm{DFT}}^{s} - \left\{ E_{\mathrm{DFT}}^{\mathrm{SQS}} - \sum_f \left[V_f^{(n)-\mathrm{fix}} + V_f^{(n)-\mathrm{rel}} \right] \xi_f^{(n)-\mathrm{SQS}} \right\}. \tag{6}$$

Those results are shown with solid red circles.

The ordering energies derived from the Ising Hamiltonian, obtained with the unified cluster expansion method

$$E_{\mathrm{Ising}}^{s-\mathrm{ord}} = \sum_f \left[V_f^{(n)-\mathrm{fix}} + V_f^{(n)-\mathrm{rel}} \right] \xi_f^{(n)-s}, \tag{7}$$

are shown with striped circles to the right of the results from the direct calculations. Lines connect the values obtained for the same structure with the two different approaches. The large spread in ordering energies, more than 0.280 eV/f.u. for structures at $x = 0.5$ and almost as much for the structures with $x = 0.75$, illustrate the strength of the configurational interactions. As compared to those values the effective cluster interactions describe the ordering energies very well, with an average magnitude of the errors of 8.8 meV/f.u.. However, an increase in the errors can be seen for the structures at $x = 0.75$, indicating the difficulties to describe the Al-richest

region, as discussed above. On the other hand, this region corresponds to compositions where the cubic phase cannot be grown experimentally any way. Noting that we can expect a slightly larger inaccuracy in the analysis of compositions with $x \geqslant 0.75$, we move on to the thermodynamics study.

V. THERMODYNAMICS OF c-TiAlN

With the effective interaction potentials of the generalized Ising Hamiltonian at hand we can start our analysis of the clustering thermodynamics of c-TiAlN. The objective is to obtain the Gibb's free energy of mixing that governs the phase stabilities. Previously, we have done so using the mean-field approximation[8,9]

$$G(x,P,T) = H^{\mathrm{MF}}(x,P) - TS^{\mathrm{MF}}(x), \tag{8}$$

where $H^{\mathrm{MF}}(x,P)$ is the mixing enthalpy of the ideal random solid solution and

$$S^{\mathrm{MF}}(x) = -k_B[xlnx + (1-x)ln(1-x)] \tag{9}$$

is the entropy of such a system. Since the completely random alloy configuration has the highest entropy, the mean-field description of the configuration becomes an excellent approximation as $T \to \infty$. At lower temperatures, short-range clustering (or ordering in other systems) will decrease the enthalpy term more than the entropy term, so the mean-field approximation overestimates the free energy and underestimates the stability of the solid solutions.

These effects can be captured with a series of canonical Monte Carlo calculations with the configurational Hamiltonian in Eq. (1). We have performed such calculations for fixed compositions with the step $\Delta x = 0.05$ over the relevant concentration range at specific temperature. Our Monte Carlo simulations are carried out using the Metropolis algorithm[31] utilizing simulations boxes of the dimension $16 \times 16 \times 16$ conventional cubic cells with 16 384 metal atoms. For each temperature we perform 13 000 trial steps per atom, of which 8000 per atom are used to collect thermodynamic data. In this work we neglect vibrational effects and consider zero-pressure conditions where the volumes used to calculate E are the equilibrium volumes for each solid solution. In this case we get

$$G(x,T) = E(x,T) - TS(x,T), \tag{10}$$

where

$$E(x,T) = E^{\mathrm{MF}}(x) + E^{\mathrm{MC}}(x,T) \tag{11}$$

$$S(x,T) = S^{\mathrm{MF}}(x) + \int_{\infty}^{T} \frac{C_V(x,T')}{T'} dT', \tag{12}$$

where $E^{\mathrm{MF}}(x)$ is the mean-field energy, while $E^{\mathrm{MC}}(x,T)$ and $C_V(x,T)$ are the energy and specific heat obtained in the Monte Carlo simulation.

We note that the Monte Carlo energy, $E^{\mathrm{MC}}(x,T)$, is negative since it is the deviation of the energy of the system from the energy of the ideal solid solution due to short-range order effects at a fixed composition. Also, the change in entropy is negative since $C_V(x,T)$ and T are both positive, while the integration goes from higher to lower temperature values. We assume that $S(x,T = 10\,000\ \mathrm{K}) \approx S^{\mathrm{MF}}(x)$ and perform the thermodynamic integration from this temperature downward to the temperature of interest. The resulting free energies of mixing, calculated both within the mean-field approximation, Eq. (8), and via the more accurate treatment from Eqs. (10)–(12), are shown in Fig. 6 for the temperature range 2000–8000 K.

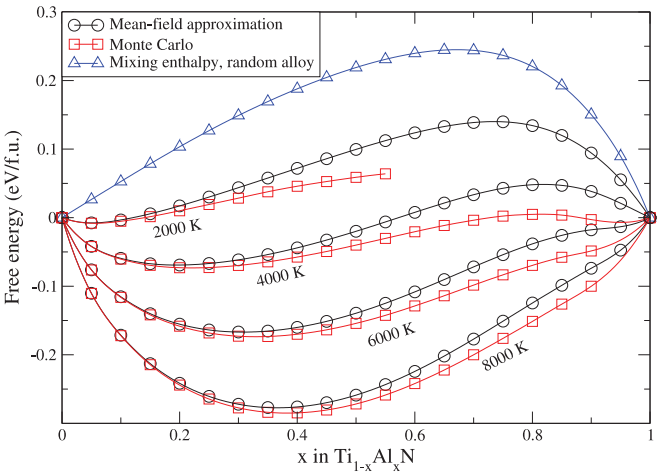

FIG. 6. (Color online) The Gibb's free energy of mixing, at zero pressure, for cubic $Ti_{1-x}Al_xN$ solid solutions as calculated with two different methods, a mean-field approximation (black circles) and Monte Carlo simulations (red squares). Values for temperatures of $T = 2000$, 4000, 6000, and 8000 K are shown together with the mixing enthalpy of the completely random solid solution.

The Monte Carlo simulations are restricted by compositions $x \leqslant 0.9$, since at higher Al concentrations the effective interactions become divergent and produce quite high error. However, this does not influence more than marginally the predictions about phase stabilities in the Ti-richer regions, which is relevant for the experimentally achievable cubic phases. The mixing enthalpy of the completely random solid solution is shown for comparison.

The equilibrium phase separation transition temperature can be determined for each composition by a common tangent construction. This temperature is higher than the corresponding phase-separation temperature in the individual *canonical* Monte Carlo simulations. This is so since in reality, and taken into account with the common tangent construction, there is always an additional energy gain for the equilibrium phase separation in comparison with the fixed volume Monte Carlo simulations. In the latter, the decomposition products are not allowed to fully relax and are kept out of equilibrium in a homogenous state to lower temperatures.

Let us note that it is difficult to perform an accurate thermodynamic integration close to the instability temperature in the Monte Carlo simulations. However, as discussed above, this is enough to determine both the binodal and, for most compositions, the spinodal lines of the phase diagram. The Monte Carlo derived free energy curve corresponding to $T = 2000$ K is shown only for compositions with $x \leqslant 0.55$ since, at this temperature, the canonical clustering temperatures have been reached for higher Al content.

At high temperatures, e.g., $T = 8000$ K, the mean-field free energy is very close to the free energy including the clustering contribution, with only a small deviation at high Al content where the effective cluster interactions become quite strong.

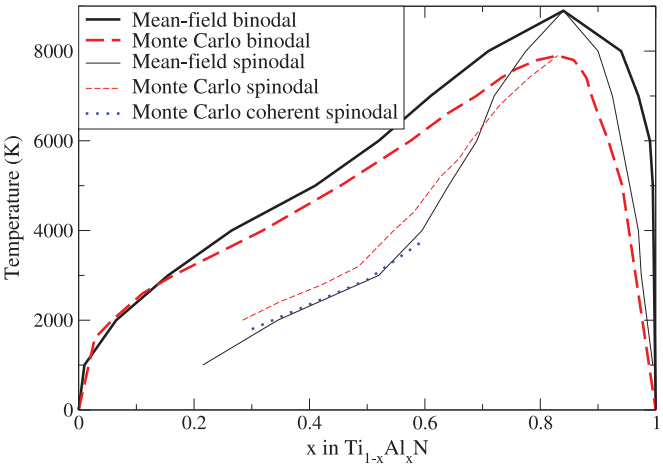

FIG. 7. (Color online) The isostructural phase diagram of cubic TiAlN as calculated with both the mean-field approximaiton, Eq. (8) (black solid lines), and the Monte Carlo approach, Eqs. (10)–(12) (red dashed lines). The binodal lines are shown with thick lines while the spinodal lines, corresponding to the condition $(\frac{\partial^2 G}{\partial x^2})_T = 0$, are shown by thin lines. The simulation of the coherent spinodal is shown with a dotted line.

As the temperature decreases, the importance of the clustering becomes more and more apparent over a larger composition range.

The phase diagram with the binodal lines derived with the common tangent construction and the spinodal lines from the consideration of the $(\frac{\partial^2 G}{\partial x^2})_T = 0$ condition is seen in Fig. 7. The Monte Carlo–derived results are actually similar to the mean-field ones, especially in the composition region $x \leqslant 0.66$, in which the single-phase cubic thin films are possible to grow experimentally.[32] In the Al-rich region, the impact of the clustering effects are somewhat larger. The maximum temperature of the miscibility gap in the mean-field approximation is 8900 K at $x = 0.84$, while the local clustering effects reduce this temperature to 7900 K at $x = 0.83$. Of course, these temperatures are of mere theoretical interest since the melting temperature of TiN is ∼3500 K[16] and the equilibrium wurtzite structure AlN should unavoidably form at temperatures well below the closure of the cubic miscibility gap. At temperatures of more practical interest for the cutting applications, $T < 1500$ K, the miscibility gap covers almost the entire composition range regardless if short-range clustering effects are considered or not.

The spinodal region, believed to be of particular importance for age hardening, also covers the larger part of the composition space. At $T = 2000$ K compositions with $x \geqslant 0.29$ are subject to spinodal decomposition according to the Monte Carlo simulations (we neglect the Al-richest side where a minimal amount of Ti could be present without spinodal decomposition at this temperature). In the Ti-rich region, $x \leqslant 0.5$, the Monte Carlo spinodal line is actually ∼500 K above the mean-field spinodal line. Since the presented results correspond to the so-called chemical spinodal, where the free energy of each composition is derived for its equilibrium volume, it is of interest to study also the coherent spinodal line, the phase region where spinodal decomposition occurs even without any possibilities for volume relaxation of the resulting phases. We estimate these temperatures for the Al content $x = 0.3$, 0.4, 0.5, and 0.6 by substituting the zero-pressure mixing enthalpies with the mixing energies calculated at the relevant fixed volume; e.g., when obtaining the coherent spinodal for $x = 0.5$, all the mixing energies entering as ΔH_{mix} in Eq. (2) or $E^{\mathrm{MF}}(x)$ in Eq. (11) are calculated at the equilibrium volume for c-$Ti_{0.5}Al_{0.5}N$. The resulting coherent spinodal is shown with a blue dotted line in Fig. 7. The difference from the chemical spinodal is a decrease in spinodal temperatures by about 400–500 K in the composition interval considered here.

There is a relatively close agreement between the phase diagram obtained with our accurate thermodynamic treatment and the approximate mean-field approach in the TiN-rich region. Our view is that for these compositions, the phase separation proceeds through a first-order phase transition, quite far from the critical point where short-range correlations, neglected completely in the mean-field approach, become important. One reason is the presence in the TiAlN system of a small, but finite, volume mismatch. The volume differences are almost entirely governed by the composition rather than by particular configurations at a fixed composition. In the AlN-rich regime the impact of short-range clustering is stronger. However, for those compositions the cubic phase diagram is of less practical interest due to the tendency to form the stable wurtzite structure of AlN.

VI. CONCLUSIONS

In conclusion, we have introduced the unified cluster expansion method and solved the difficult alloy problem of clustering thermodynamics in c-$Ti_{1-x}Al_xN$. This approach illustrates how the two main tools of alloy theory to obtain effective cluster interactions, the structure inversion and the generalized perturbation methods, could be fruitfully combined. We do so by separating the interactions into chemical contribution obtained on a fixed lattice, for which the GPM method works well, and the lattice relaxation term, for which the cluster expansion is applied. Using these interactions we perform Monte Carlo simulations to determine the short-range clustering effects on the free energy of mixing. When constructing the isostructural phase diagram we find that cubic TiAlN is a phase-separating system over almost the whole concentration range at typical cutting tool working temperatures $1000 \leqslant T \leqslant 1500$ K. At $T = 2000$ K the spinodal region extends from about $x \geqslant 0.33$ or $x \geqslant 0.28$, depending if one considers coherent decomposition conditions. The results show a striking, but explainable, close resemblance with those obtained with the mean-field approximation in the composition region of experimental and industrial relevance.

ACKNOWLEDGMENTS

The Swedish Research Council (VR), the Swedish Foundation for Strategic Research (SSF), and the Göran Gustafsson Foundation for Research in Natural Sciences and Medicine are acknowledged for financial support. Calculations were performed using computational resources allocated by the Swedish National Infrastructure for Computing (SNIC).

*bjoal@ifm.liu.se

[1]G. Beensh-Marchwicka, L. Kròl-Stepniewska, and W. Posadowski, Thin Solid Films **82**, 313 (1981).
[2]O. Knotek, M. Böhmer, and T. Leyendecker, J. Vac. Sci. Technol. A **4**, 2695 (1986).
[3]W. D. Münz, J. Vac. Sci. Technol. A **4**, 2717 (1986).
[4]P. H. Mayrhofer, C. Mitterer, L. Hultman, and H. Clemens, Prog. Mater. Sci. **51**, 1032 (2006).
[5]P. H. Mayrhofer, A. Hörling, L. Karlsson, J. Sjölén, T. Larsson, C. Mitterer, and L. Hultman, Appl. Phys. Lett. **83**, 2049 (2003).
[6]A. E. Santana, A. Karimi, V. H. Derflinger, and A. Schutze, Tribol. Lett. **17**, 689 (2004).
[7]P. H. Mayrhofer, D. Music, and J. M. Schneider, Appl. Phys. Lett. **88**, 071922 (2006).
[8]B. Alling, A. V. Ruban, A. Karimi, O. E. Peil, S. I. Simak, L. Hultman, and I. A. Abrikosov, Phys. Rev. B **75**, 045123 (2007).
[9]B. Alling, M. Odén, L. Hultman, and I. A. Abrikosov, Appl. Phys. Lett. **95**, 181906 (2009).
[10]D. Holec, F. Rovere, P. H. Mayrhofer, and P. B. Barna, Scripta Mater. **62**, 349 (2010).
[11]F. Ducastelle, *Order and Phase Stability in Alloys* (North-Holland, Amsterdam, 1991).
[12]P. H. Mayrhofer, D. Music, and J. Schneider, J. Appl. Phys. **100**, 094906 (2006).
[13]F. Ducastelle and F. Gautier, J. Phys. F **6**, 2039 (1976).
[14]J. W. D. Connolly and A. R. Williams, Phys. Rev. B **27**, 5169 (1983).
[15]C. R. Houska, J. Phys. Chem. Solids **25**, 359 (1964).
[16]H. A. Wriedt and J. L. Murray, Bull. Alloy Phase Diagrams **8**, 378 (1987).
[17]L. Vitos, I. A. Abrikosov, and B. Johansson, Phys. Rev. Lett. **87**, 156401 (2001).
[18]L. Vitos, Phys. Rev. B **64**, 014107 (2001).
[19]P. E. Blöchl, Phys. Rev. B **50**, 17953 (1994).
[20]G. Kresse and J. Furthmüller, Phys. Rev. B **54**, 11169 (1996).
[21]G. Kresse and D. Joubert, Phys. Rev. B **59**, 1758 (1999).
[22]A. Zunger, S. H. Wei, L. G. Ferreira, and J. E. Bernard, Phys. Rev. Lett. **65**, 353 (1990).
[23]I. A. Abrikosov, S. I. Simak, B. Johansson, A. V. Ruban, and H. L. Skriver, Phys. Rev. B **56**, 9319 (1997).
[24]A. V. Ruban and I. A. Abrikosov, Rep. Prog. Phys. **71**, 046501 (2008).
[25]G. Ghosh, A. van de Walle, and M. Asta, Acta Mater. **56**, 3202 (2008).
[26]J. P. Perdew, K. Burke, and M. Ernzerhof, Phys. Rev. Lett. **77**, 3865 (1996).
[27]A. V. Ruban and H. L. Skriver, Phys. Rev. B **66**, 024201 (2002).
[28]A. V. Ruban, S. I. Simak, P. A. Korzhavyi, and H. L. Skriver, Phys. Rev. B **66**, 024202 (2002).
[29]A. V. Ruban, S. Shallcross, S. I. Simak, and H. L. Skriver, Phys. Rev. B **70**, 125115 (2004).
[30]I. A. Abrikosov, A. M. N. Niklasson, S. I. Simak, B. Johansson, A. V. Ruban, and H. L. Skriver, Phys. Rev. Lett. **76**, 4203 (1996).
[31]N. Metropolis, A. W. Rosenbluth, M. N. Rosenbluth, A. H. Teller, and E. Teller, J. Chem. Phys. **21**, 1087 (1953).
[32]A. Hörling, L. Hultman, M. O. J. Sjölen, and L. Karlsson, Surf. Coat. Technol. **191**, 384 (2005).